
# Multiphase photo-capillary reactors coated with $TiO_2$ films: preparation, characterization and photocatalytic performance

L. Hurtado, D. Solís-Casados, L. Escobar-Alarcón, R. Romero, R. Natividad

PII: S1385-8947(16)30810-5
DOI: http://dx.doi.org/10.1016/j.cej.2016.06.003
Reference: CEJ 15313

To appear in: *Chemical Engineering Journal*

Received Date: 1 April 2016
Revised Date: 27 May 2016
Accepted Date: 1 June 2016

Please cite this article as: L. Hurtado, D. Solís-Casados, L. Escobar-Alarcón, R. Romero, R. Natividad, Multiphase photo-capillary reactors coated with $TiO_2$ films: preparation, characterization and photocatalytic performance, *Chemical Engineering Journal* (2016), doi: http://dx.doi.org/10.1016/j.cej.2016.06.003

# Multiphase photo-capillary reactors coated with $TiO_2$ films: preparation, characterization and photocatalytic performance

L. Hurtado[1], D. Solís-Casados[1], L. Escobar-Alarcón[2], R. Romero[1], R. Natividad[1*]

[1]Centro Conjunto de Investigación en Química Sustentable, UAEMex-UNAM, Universidad Autónoma del Estado de México, km 14.5 Toluca-Atlacomulco Road, 50200 Toluca, Mexico

[2]Departamento de Física, Instituto Nacional de Investigaciones Nucleares, Mexico

*Corresponding author contact. E-mail: reynanr@gmail.com. Telephone: +52 722 2766610 ext. 7723

Abstract

Quartz capillaries were assessed as multiphase photocatalytic reactors. The tested reaction was the salicylic acid (2-dihidroxibenzoic acid) oxidation. The catalyst ($TiO_2$) was either in slurry or immobilized by sol-gel method onto the capillary wall. All experiments were conducted under oxygen flow and Taylor flow hydrodynamic regime. $TiO_2$ Films were characterized by Raman spectroscopy, diffuse reflectance UV-Vis spectroscopy and scanning electronic microscopy. The effect of two synthesis variables was established. These variables were volumetric ratio of precursors solutions (i-PrO:2-propanol:nitric acid) and number of capillary coating cycles. These variables were found to importantly affect film homogeneity and oxidation rate. The highest initial reaction rate ($106.32 \times 10^{-6}$ mol $dm^{-3}s^{-1}$) was obtained when using the $TiO_2$ as film prepared with a precursors volumetric ratio of 1:15:1 and with two coating cycles. For comparison purposes, the same oxidation process was conducted in a stirred reactor and it was found that the reaction rate value is diminished by almost four times in comparison with that obtained under Taylor flow in the capillary reactor. Selectivity was found to be dependant on the type of catalyst addition, slurry or immobilized. Catalytic films employed in this non-common reaction system were

reused three times losing less than 10% of their photocatalytic activity. The photonic efficiency was found to be two orders of magnitude higher in the coated capillary reactor than in the slurry stirred reactor.
Keywords: photocatalysis, $TiO_2$, 2-hidroxibenzoic acid, Taylor flow, catalyst immobilization

## 1. Introduction

Heterogeneous photocatalysis has been recognized as an advanced oxidation process (AOP) able to successfully degrade and mineralize a wide range of toxic organic compounds [1-4]. Nevertheless, in the last decade and in the context of green chemistry, special attention has been given to photocatalytic processes to conduct selective photocatalyzed oxidation reactions [5, 6]. In either type of photocatalytic processes, advanced or selective oxidation, the essential components are the catalyst, the radiation source, the chemical compound to be degraded and the photoreactor. In this sense, there are various plausible reactor configurations reported in literature, most of them aiming at maximizing photonic efficiency. This efficiency depends on the parameters affecting reaction rate, the incident radiation and the surface illuminated per volume inside the reactor [7]. Therefore, by changing the catalyst type and concentration, reagents concentration and the irradiated area and volume, the photonic efficiency can be tuned.

In this context, capillary reactors are expected to be efficient for photocatalytic applications due to a higher illuminated surface area, lower pressure drop, functionalized surfaces as well as improved mass and heat transfer compared to traditional batch reactors [8, 9]. The great performance in mass and heat transfer in capillary channels are based on their specific hydrodynamics characteristics. Regarding this feature, different flow patterns have been observed inside a capillary channel, for example annular, bubbly, churn, and slug or also called Taylor flow. This type of flow consists of an arrangement of elongated bubbles and liquid *slugs.* It has been reported that the hydrodynamics of this flow pattern improves the mass transfer due to the thin layer of liquid formed between the gas phase and the wall of the channel, minimizing the resistance to mass transfer [10]. Also, the phenomena in one capillary can be extrapolated to a bunch of capillaries [11, 12]. This makes the scaling up of a process conducted in a

capillary reactor relatively easier than one performed in a typical stirred tank reactor. Albeit the attractive features of capillary reactors and Taylor flow, their application to heterogeneous photocatalytic processes is rather scarce. Thus, this work aims to assess the performance of such technology (multiphase capillary reactors) in photocatalysis. This was conducted with $TiO_2$ in slurry and immobilized as a film onto the capillary reactor wall. It is well known that $TiO_2$ is an efficient photocatalyst and exhibits a high oxidative power, high stability, low cost and relatively low toxicity [13]. It is very common to use $TiO_2$ powder in photocatalytic processes due to its large surface area/volume ratio which improves the photocatalytic efficiency. However, the use of a slurry catalyst implies an additional step in the process, i.e. separate and recover catalyst from reaction media. In order to address this issue an alternative route is to immobilize the catalyst onto a suitable support as a thin film. Albeit the existent catalytic thin film preparation methods (chemical vapor deposition [14], chemical spray pyrolysis [15], pulsed laser deposition [16] and sol–gel method [17, 18]), in this work we use the sol–gel method since it was considered the most suitable one from a geometric point of view.

The elected model molecule to assess the performance of the proposed multiphase photo-reaction system was salicylic acid or also called 2-dihidroxibenzoic acid (2-DHBA). This molecule is considered as representative of the soluble aromatic compounds and possesses both, intramolecular and intermolecular hydrogen bonds (see Figure 1) [19]. In addition, the reported salicylic acid degradation mechanism [20] suggests a number of parallel and consecutive reactions. This type of mechanism is desirable to assess the versatility of the proposed reaction system to tune products distribution.

FIGURE 1

## 2. Experimental methods

### *2.1 Reagents*

Titanium (IV) isopropoxide (i-PrO) $Ti[OCH(CH_3)_2]_4$ (97%) was purchased from Sigma-Aldrich. 2-propanol $CH_3CHOHCH_3$ and nitric acid $HNO_3$ (70%) were purchased from Fermont. 2-dihidroxibenzoic acid (2-DHBA), 2,3-dihidroxibenzoic acid (2,3-DHBA), 2,5-dihidroxibenzoic acid (2,5-DHBA) and orto-phosporic acid (85% in aqueous solution) were supplied by Sigma-Aldrich. Potassium phosphate ($K_3PO_4$) and methanol HPLC degree were purchased from Fermont. Deionized water was employed at all experiments. All chemicals were used as received without further purification except the mobile phase for HPLC analysis. Quartz rounded capillaries with inner diameter of 0.003 m, 0.001 m thickness and 0.2 m length were employed as substrates.

### *2.2 Thin films preparation*

Capillary-channels were washed, rinsed with distilled water and dried at 150 °C for 2 hours before impregnation of precursors of $TiO_2$ by sol-gel method. Quantities of precursors were selected according to the desired properties of the thin films. The first studied synthesis variable was the alkoxide:alcohol ratio. For this purpose, solutions with volumetric ratios of i-PrO:2-propanol:nitric acid equal to 1:5:0.5,1:10:1, 1:15:1, 1:20:1 and 1:50:1, were prepared. Once the optimal precursors ratio was established according to photocatalytic performance on 2-dihidroxibenzoic acid degradation, the next step was to determine the number of coating cycles that leads to the highest degradation rate of the model molecule. The tested number of coating cycles were 1, 2 and 3. Regarding films preparation, alcohol and isopropoxide were mixed in a glass beaker and finally nitric acid was dropwise added. Precursors solution was kept under magnetic stirring for 4 hours at 800 rpm avoiding contact with air. Once the precursor sol was homogenized, dried substrate was completely immersed in a receipt containing sol phase during 60 seconds and thrown out. The resulting film outside the channel was taken away. After impregnation, the substrates were calcined at 450°C for 5 hours at a heating rate of 10 °C per minute and finally cooled down to room temperature.

### 2.3 Films characterization

The resulting $TiO_2$ films were characterized by scanning electron microscopy (SEM) and Raman (RS) and UV-Visible spectroscopies. The Raman spectra were acquired using an HR LabRam 800 system equipped with an Olympus BX40 confocal microscope. SEM images provided information about the morphology of samples and were obtained with a JEOL microscope (Model JSM-6510LV) equipped with an Oxford INCA Penta FETx3 EDS system. Values of band gap energy and film thickness were estimated by using the Tauc and Goodman method respectively from UV-Vis spectra obtained with a Perkin Elmer Lambda 35 UV-Vis spectrometer equipped with a Labsphere RSA-PE-20 integrating sphere of 50 mm of diameter. The material used as reference was Spectralon.

### 2.4 Reaction set-up and chemical analysis

The capillary reaction system is shown in Figure 2 and it was configured as follows: capillary channel with internal coating of $TiO_2$ worked as reaction zone. Inlets of liquid and gas phases were placed in a "T" junction located at the top of the channel. Liquid phase consisted of an aqueous solution of 2-DHBA [100 ppm] and was introduced to the system driven by a peristaltic pump (Cole-Parmer model 7553-30) from the reservoir vessel containing 45 mL at the beginning of the experiment, the pump head selected was a Masterflex 7016-20 with a silicon tubing L/S 16. Gas phase was oxygen provided directly from the cylinder (Infra 99.5%) and the entrance flow was regulated by a mass flow controller (Aalborg GFC17). Liquid deposit was kept under constant temperature of 35°C by employing a water bath. Due to the strong influence of the reological properties of working fluids over the Taylor flow pattern, it was explored an interval of temperature of the liquid between 25 and 40 °C and it was found that 35°C was the temperature which offers a better control and stability of the flow pattern. Temperature was continuously measured with a temperature sensor (Conductronic STD11MonoB11). The source of radiation consisted of a UVP-Pen Ray lamp model 3SC-9. This mercury lamp possesses its main emission at 254 nm. Irradiation flux

was determined with a UVP® radiometer model UVX equipped with an UV sensor (254 nm). The lamp was located next to the channel at a distance of 0.002 m from the external wall of the capillary reactor and with this configuration, the photonic flux inside the channel was determined to be 3.92 mW $cm^{-2}$. Prior photo-reaction, liquid and gas velocities were regulated until the Taylor flow-pattern was observed. The amount of catalyst per liter of solution inside the coated capillary reactor was determined to be 1.43 g $L^{-1}$. Additional experiments were conducted to determine the effect of adding oxygen rather than air and to establish whether or not Taylor flow favours oxidation over bubbly flow. Samples were withdrawn from the liquid reservoir periodically for chemical analysis. Control experiments included adsorption and photolysis. Also, the effect of hydrodynamics on conversion and selectivity was studied by conducting the reaction not only in a capillary reactor but also in a stirred tank reactor. The experiment conducted in a stirred tank reactor was performed by placing 45 mL of 2-DHBA acid solution [100 ppm] and $TiO_2$ Degussa P25 (catalyst concentration equal to 0.5 g $L^{-1}$) in a flask which also was equipped with an oxygen distributor at the bottom. This catalytic suspension was kept at 35°C and under magnetic stirring (800 rpm) until the end of the experiment. Oxygen was bubbled continuously at a flow equal to 20 mL $min^{-1}$ to attain Taylor flow. For selected experiments the dissolved oxygen concentration was determined by a dissolved oxygen portable meter from HACH (HQ 40d). The employed radiation source was the same previously described for the capillary reactor and in this case was placed inside the suspension at the centre of the flask. The photonic flux inside this reactor was determined to be 7.56 mW $cm^{-2}$. For samples of catalytic suspensions, prior to analysis it was necessary to separate the powder by centrifugation at 10,000 rpm during 10 minutes.

Degradation of the 2-DHBA molecule was established by UV-Vis spectroscopy in a HACH 5000 equipment following the absorbance change at 299 nm. The molecule mineralization degree at the end of the photocatalytic process was established by Total Organic Carbon (TOC) analysis by employing a Shimadzu TOC-$L_{CPN}$ device. Furthermore, the main reaction intermediates were identified and quantified by high performance liquid chromatography in a HPLC Waters 1015 equipment operating in isocratic

mode with a Sigma-Aldrich® Discovery C18 column at room temperature. Mobile phase composition was determined to be $K_3PO_4$ buffer:Methanol in a 65:35 ratio. Buffer pH was adjusted to 2.5 with ortho-phosporic acid prior to be mixed with methanol. The mobile phase flow was kept constant (1.35 ml $min^{-1}$) during analysis. The UV detector of the equipment was configured to 299 nm for 2-DHBA and 315 nm for 2,3-DHBA and 2,5-DHBA.

FIGURE 2

## 3. Results and discussion

### *3.1 Thin films characterization*

#### *3.1.1 Morphology*

The inner wall of quartz capillaries was coated with $TiO_2$ films as is revealed by the microscopies showed in Figure 3. These are representative of different films obtained depending on synthesis conditions. In all of them, the deposited film over the quartz wall is evident. However, there are remarkable differences that depend on the precursors dilution degree. By increasing the alcohol:alcoxide ratio, the transparency in the obtained films was considerably higher. This fact was initially desirable due to the photocatalytic application. On the other hand, however, it was found that the low thickness of the film likely is related to the partial or complete separation from the substrate resulting in low photocatalytic activity. Three representative cases of the degree of dilution are presented. When films were prepared with the volumetric ratio of the *sol* precursor (i-PrO:2-propanol:$HNO_3$) equal to 1:5:0.5 (Figure 3, A), lumps of approximately 100 μm were observed over the main film. Additionally, an important degree of cracking in the film was also detected. The next studied volumetric ratio was 1:25:1 (Figure 3, B). In this case, cracks in the film were also detected, although the formation of lumps was discarded given the higher solubility of the precursor sol. Finally, the volumetric ratio equal to 1:50:1 (Figure 3, C) allowed the formation of films

without lumps neither considerable breakages on the surface (size<5 μm). Furthermore the opacity of the film was considerably diminished in comparison with more concentrated preparations. These differences were definitely expected to have an impact on catalytic performance and this will be discussed in another section. Meanwhile, the characterization results presented here will be focused on the films prepared with the volumetric ratio equal to 1:15:1 due to its higher photocatalytic activity in the degradation and mineralization of 2-DHBA. Figure 4 presents a typical micrography of as-prepared quartz substrate internally covered with $TiO_2$ with a volumetric ratio of 1:15:1 exposed to two dip-coating and calcination cycles. As one can see, the film is mainly conformed by a regular coating without excessive lumps or fractures. Also, it is worth noticing that the film was not damaged by cutting the capillary to obtain this image indicating that the film was strongly adhered to the wall because of the sol acidity (pH<2) used.

FIGURE 3

FIGURE 4

### *3.1.2 Raman spectroscopy*

Microstructure characterization of films performed by Raman spectroscopy confirms the deposit of $TiO_2$ over the surface of substrates. The Anatase phase was identified as the only $TiO_2$ crystalline phase characterized by five active Raman modes peaking at 144, 197, 397, 513 and 637 $cm^{-1}$, as is shown in Figure 5. The most intense signal appears at 144 $cm^{-1}$ and is characteristic of anatase phase. Table 1 summarizes the point group symmetry corresponding to the band assignation reported by Karthik *et. al.* [21].

Table 1. Active Raman modes of anatase phase of $TiO_2$

| Location | Point group Symmetry |
|---|---|
| 144 $cm^{-1}$ | $E_g$ |
| 197 $cm^{-1}$ | $E_g$ |
| 399 $cm^{-1}$ | $B_{1g}$ |
| 513 $cm^{-1}$ | $A_{1g}$ |
| 639 $cm^{-1}$ | $E_g$ |

In Figure 5, a slight displacement and changes on intensities of the peak at 144 $cm^{-1}$ can be observed. This could be attributed to variations in composition of the precursor sol. It was found that for a less diluted precursor sol (1:5:0.5) the signals are clearly identified. As dilution increases, however, the Raman intensity decreases and the bands at higher frequencies almost disappear and only the signal corresponding to 144 $cm^{-1}$ is noticeable. Additionally, at the higher dilutions a broad band peaking around 450 $cm^{-1}$, attributed to the quartz substrate, is clearly seen. This result suggests films with lower thicknesses as the dilution increases. This fact is expected since the growing of films is strongly influenced by dilution degree as has been previously shown by SEM images albeit our main interest was to keep cristallyne phase of $TiO_2$ in order to explain the influence of precursor sol over photocatalytic activity. Despite the vast literature regarding Raman spectroscopy for $TiO_2$ samples, the study of structural characterization of thin films is limited but an interesting fact is provided by Xu and co-workers [22]. In such a study, the Ti-O stretching modes normal to the film plane, $A_{1g}$+$B_1$, are suppressed due to dimensional limitations in the film plane. The suppression of these vibration modes means that the film has a very low thickness. This fact may help to explain the reason to observe only four typical bands of anatase phase in our samples instead of five.

FIGURE 5

### *3.1.3 Optical characterization*

Since the application of thin films is related to photocatalytic processes, we consider essential to characterize them from the optical perspective; specifically, estimation of film thickness, refractive index and band gap energy. For the first two parameters, the optical interference Goodman method for the approximate determination of a transparent layer on a transparent substrate was selected [23]. The required experimental information is obtained from a single spectrophotometric study recording transmittance of the catalytic film and its substrate (see Figure 6). It must be considered that the film and the substrate are assumed to be nondispersive over the wavelength region of interest.

FIGURE 6

Thus, for refractive index estimation of thin films, equation [1] must be evaluated:

$$n_{film} = \left\{ \frac{-(n_0^2 + n_2^2)(1 - 2\rho_{T2}) + \left[(n_0^2 + n_2^2)^2 (1 - 2\rho_{T2})^2 - 4n_0^2 + n_2^2\right]^{1/2}}{2} \right\}^{1/2} \quad \text{Eq. [1]}$$

$$\rho_{T2} = \frac{T_{MAX}}{T_{MIN}} \quad \text{Eq. [2]}$$

Where:

$n_{film}$: refractive index of thin film

$n_0$: refractive index of medium (air, 1.0)

$n_2$: refractive index of substrate (glass, 1.5)

Furthermore, once the refractive index of films was estimated, equation [3] was employed to estimate the film thickness ($t$),

$$t = \frac{M_{ab}\lambda_a\lambda_b}{2(\lambda_a - \lambda_b)(n_p^2 - \sin^2\theta_0)^{1/2}} \qquad \text{Eq. [3]}$$

where:

$n_{film}$: Refractive index of thin film

$\lambda_a$: Wavelenght corresponding to maximum transmittance

$\lambda_b$: Wavelenght corresponding to minimum transmittance

$M_{ab}$: Number of max. and min. between $\lambda_a$ and $\lambda_b$.

$\theta_0$: Light incident angle

Summarizing, the optical parameters of the $TiO_2$ film synthesized with a volumetric precursors ratio equal to 1:15:1 and two coating cycles was estimated to be $n_{film}=1.5$ and $t=560$ *nm.* The thickness of 560 nm is certainly large compared to those reported in literature for thin films although most of them were prepared by chemical methods. A few examples are the $TiO_2$ films of 225±14 nm thickness reported by Solis [18] prepared by spin coating and the $TiO_2$ film of 100 nm thickness prepared by Mohamed [24] by electron beam evaporation. It should be bear on mind that in this study dip coating was selected as coating technique due to the large area to cover (6 x$10^{-4}$ $m^2$) and the complexity to cover a round and large inner wall by rather sophisticated procedures. Nevertheless the broad thickness, the transmittance is around 50% in the wavelength of interest and losses in transparency of the films are compensated by strong adherence of the film to the substrate. This is highly desirable for photocatalytic purposes in continuous operation.

In addition, the band gap energy of the synthesized $TiO_2$ films was evaluated. Again, from the transmittance spectrum, the band gap energy was determined according to the Tauc plot method reported

elsewhere [25] This was performed by plotting $(\alpha h\upsilon)^{1/2}$ as function of the photon energy (Figure 7) and then by a linear regression of the linear part corresponding to the absorption edge region of the film. The calculated band gap energy was 3.2 eV in very good agreement with the value reported for the anatase phase of $TiO_2$ [26].

FIGURE 7

*3.2 Flow patterns mapping*

Prior testing the photocatalytic activity of the prepared films, it was necessary to identify the operational window of Taylor flow. This makes necessary the introduction of two dimensionless groups, i.e.Capillary (Ca) and Reynolds (Re) numbers which are given by the following expressions (adapted from [10]):

$$Ca = \mu u_{TP}/\gamma \qquad \text{Eq. [4]}$$

Where:

$Ca$: Capillary number

$\mu$: Viscosity (Pa s)

$u_{TP}$: Velocity of two phases (m $s^{-1}$)

$\gamma$: Surface tension (N $m^{-1}$)

And:

$$Re = D\rho u_{TP}/\mu \qquad \text{Eq. [5]}$$

Where:

$Re$: Reynolds number

$D$: Capillary diameter (m)

$\rho$: Density (kg $m^{-3}$)

$u_{TP}$: Velocity of two phases (m $s^{-1}$)

$\mu$: Viscosity (Pa s)

A set of experiments for the system 2-DHBA-$O_2$ in which velocities of liquid and gas phase were varied was performed in order to establish flow regions in which bubble, Taylor and annular patterns are achieved and the results are shown in Figure 8 as function of dimensionless groups.

FIGURE 8

Flow patterns are clearly defined and for the specific case of Taylor flow can be developed in the following intervals: $20<Re<100$ and $1x10^{-4}<Ca<4x10^{-4}$.

*3.3 Photocatalytic activity*

In order to assess the performance of the multiphase capillary reactor in photo-oxidation reactions, the oxidation of 2-DHBA was selected. Liquid and gas flowrates were varied until Taylor flow was observed. Among flow patterns in capillary channels, we focused on Taylor flow because of its benefits regarding mass transfer due to its hydrodynamics. Figure 9 presents typical absorbance spectra of reaction samples.

FIGURE 9

In these spectra two main absorption bands can be distinguished. The absorption band with a maximum at 299 nm is characteristic of 2-DHBA and was employed to establish this molecule concentration at initial

and close to initial conditions in order to calculate de initial reaction rates reported in table 2. The relationship of this band with the presence of aromatic rings is well known and therefore the loss of intensity likely indicates the rupture of the aromatic ring in the 2-DHBA molecule. The identification of intermediates was conducted by HPLC analysis and selectivity results are presented in the final section of this work.

The first response variable was the dilution degree of precursor sol. Five different concentrations were tested. Every capillary received two coating cycles and the differences in photocatalytic activity in terms of initial reaction rate of 2-DHBA oxidation presented in Figure 10 and summarized in Table 2. In addition, mineralization percentage after 120 minutes of irradiation is also presented in Table 2. Experimental data for each point was replicated until a difference between values obtained was ≤2%. All experiments were performed under Taylor hydrodynamic regime. Length of elongated bubbles and slugs was approximately 4±0.5 cm.

FIGURE 10

It is widely accepted that the photocatalytic oxidation of 2-DHBA molecule is strongly influenced by the catalytic surface properties [20, 27], it means, the ability of the material to generate electron-hole pairs is directly related to the $OH^{\bullet}$ radical formation that acts as oxidizing agent in the process. Initially, the molecule is adsorbed on the catalytic surface and by means of hydroxyl radical attack is decomposed to intermediates and finally to carbon dioxide and water. In this way, it was expected to find differences in photocatalytic performance as the dilution was varied. The effect of sol dilution degree on 2-DHBA initial oxidation rate is presented in Figure 10. It can be observed that the maximum initial reaction rate (106.32 x $10^{-6}$ mol $dm^{-3}$ $s^{-1}$) is obtained when the volumetric proportion is equal to 1:15:1 and this point represents the synthesis conditions that provide the balance between titanium dioxide deposited over a substrate and the transparency of the film required to ensure that UVC light goes inside the reactor. At both sides of this

point the photocatalytic performance is diminished. Firstly, when the precursor sol is quite concentrated or on the other hand, when the dilution increases. This can be attributed to the quantity of active sites being too low when dilution increases. On the other hand, the drawback of a very concentrated sol is the low transparency inhibiting transmittance of light to the reactor and as consequence, the photo-oxidation processes become restricted.

Table 2. Effect of sol precursor composition on 2-DHBA initial oxidation rate and mineralization degree

| Volumetric Proportion | $-r_{AS0}x10^6$ (mol*dm$^{-3}$*s$^{-1}$) | % Mineralization (t=120 min.) |
|---|---|---|
| 1:5:0.5 | 34.20 | 4 |
| 1:10:1 | 68.90 | 9 |
| 1:15:1 | 106.32 | 12 |
| 1:20:1 | 50.45 | 6.3 |
| 1:50:1 | 17.45 | 4 |

The results shown in Table 2, suggest the existence of an optimum value of the precursors volumetric ratio for film synthesis and is directly related to the volume of alcohol added to the sol. Regarding the mineralization of model molecule, the percent is reported as the difference between initial and final total organic carbon in samples. For this response variable the differences among them are not really drastic, however, it is evident the existence of a maximum point corresponding to 12% when the film was prepared with a ratio equal to 1:15:1. The small degree of mineralization suggests this type of reactors might be an alternative to conduct selective photo-oxidation reactions. In addition, photolysis and adsorption experiments were conducted to ensure the photocatalytic effect presented here by using $TiO_2$ films. Also, in order to establish whether or not there was an effect of hydrodynamic regime and oxygen concentration, two further experiments were conducted. One experiment was with oxygen but under

bubbly flow and the other one was under Taylor flow but with air rather than with oxygen. The obtained results are summarized in table 3. By observing these results, it can be concluded that the 2-DHBA is not removed by adsorption and that the concentration of oxygen is important to increase both, the removal and mineralization percentages of 2-DHBA.

Table 3. Effect of hydrodynamic regime and dissolved oxygen concentration on 2-DHBA removal and mineralization percentages. Reaction time= 120 minutes.

| ***Experiment*** | ***% Removal*** | ***% Mineralization*** | ***Dissolved $O_2$ (mg $L^{-1}$)*** |
|---|---|---|---|
| Adsorption | 1 | ___ | ___ |
| Photolysis | 3.6 | ___ | ___ |
| UV light+$O_2$ | 5.5 | ___ | ___ |
| Bubbly flow (with $O_2$) | 3.7 | 1.2 | 5.73 |
| Taylor flow (3.5 cm, $O_2$) | 19.2 | 12 | 7.97 |
| Taylor flow (3.5 cm, aire) | 6.7 | 1.2 | 5.15 |

The influence of the number of coating cycles on the oxidation of 2-DHBA was also tested. The number of coating cycles was varied between 1 and 3. It can be observed in Figure 11 that the best performance in terms of initial oxidation rate is given by the intermediate value (2 cycles). For only one cycle is likely that the film is not completely distributed over the substrate thus limiting the oxidation process. On the other hand, when the capillary channel receives three coating cycles, albeit the amount of titanium dioxide is expected to be higher than when the capillary is coated only once or twice, the results shown in Figure 11 suggests that light does not penetrate as effectively as when the capillary was coated only twice. Therefore, it can be concluded that a balance between number of active sites and transmittance of light should be kept in order to attain a maximum of photo-reaction rate.

FIGURE 11

It is worth pointing out that coating an inner, round and large wall is not an easy task and here we found an opportunity area for future work in order to improve reproducibility from synthesis to synthesis. By now, we can affirm that the process employed and described before accomplish the goal to successfully perform photocatalytic oxidation of a given molecule in a better way that in a classical batch reactor: the photocatalytic performance is increased by 3.7 times when the 2-DHBA oxidation process is conducted in capillary reactor instead a batch one. Figure 12 shows a comparative of initial reaction rate of 2-DHBA degradation in three different reaction system configurations: The stirred tank reactor (STR) employing $TiO_2$ Degussa P25 suspension as catalyst, the capillary reactor with slurry catalyst and finally the slurry reactor with catalytic film. Among these particular cases, the better performance is reached when the catalytic film is employed. Regarding to the advantages of catalytic films versus slurry catalyst, we found that beyond the highest photocatalytic performance, a coated capillary can be used at least three times in separate experiments and the loss of photocatalytic activity is less than 10% (For precursors volumetric rate equal to 1:15:1). This fact is clearly desirable because by only washing channels they can be reused without additional procedures. Furthermore, the step of filtration and/or centrifugation to separate catalytic powders is not necessary when $TiO_2$ films are used. The higher photocatalytic performance obtained in a capillary reactor versus stirred tank reactor is also influenced by the illuminated surface per unit of volume inside the reactor and in this sense it was found that for a capillary reactor this ratio is equal to 1346 $m^2m^{-3}$ while for a stirred tank reactor, this ratio becomes only 146 $m^2m^{-3}$. These values definitely impact the photonic efficiency. This was calculated for the three reaction systems according to the procedure described by Schneider *et. al.*[7]:

$$\xi = \frac{\langle r \rangle_{V_{reactor}} * V_{reactor}}{q_0 * A_{irr}} \qquad \text{Eq. [6]}$$

Where,

$\xi$: Photonic efficiency

$\langle r \rangle_{V_{reactor}}$: Initial reaction rate of 2-DHBA oxidation

$q_0$: Incident radiation flux

$V_{reactor}$: Reaction volume

$A_{irr}$: Irradiated area

The incident irradiation was determined to be $1.6041 \times 10^{-8}$ mol $cm^2$ $s^{-1}$ by a radiometric procedure. The calculated photonic efficiency values have been plotted in Figure 12. It can be observed that the use of a capillary reactor allows to increase up to one order of magnitude the photonic efficiency compared to a stirred tank reactor when using the same catalyst concentration. It can also be observed that a further increase on photonic efficiency is attained when the catalyst is on the capillary reactor wall. It is worth noticing that the latter allows a higher amount of catalyst per liter of liquid inside the reactor (about three times more). Nevertheless, the coated capillary reactor is characterized by backside illumination. This implies that the charge carriers are generated relatively far from the liquid-catalyst interface and, consequently, are more susceptible to recombination losses.

FIGURE 12

Also the photocatalyst reactivity in combination with the photoreactor was calculated and the values are summarized in table 4. It can be observed that the photocatalyst reactivity is higher in the coated capillary reactor than in the slurry capillary reactor.

Table 4. Effect of photo-reactor on photocatalyst reactivity

| ***Photo-reactor*** | ***Photocatalyst reativity*** | |
|---|---|---|
| | ***(mol illumin $m^{-3}$ $s^{-1}$)*** | ***(mol $kJUV^{-1}$ $m^{-3}$)*** |
| Slurry STR | 0.02877 | 0.3382 |
| Capillary (slurry) | 5.26e-4 | 0.3973 |
| Capillary (film) | 9.97e-4 | 6.99 |

As the concluding step of this work, selectivity results are shown in Figure 13. The plotted values were obtained with the intermediates concentrations calculated from HPLC analysis. It can be observed that the main formed products of 2-DHBA degradation were 2,5-DHBA and 2,3-DHBA. The product distribution, however, depends on the operating mode of the capillary reactor: slurry o immobilized catalyst. When catalyst is in slurry (0.5 g $L^{-1}$ of $TiO_2$ Degussa P25), the main product is 2,5-DHBA while the immobilized catalyst favours the formation of 2,3-DHBA. This can be ascribed to the different hydrodynamics under which the oxidation of 2-DHBA occurs. In the slurry mode, the reaction occurs within the liquid slugs. Within these slugs, a perfect mixing is expected [7]. This mixing also favours the oxygen mass transfer from the oxygen elongated bubbles to the solution (see table 3). When the reaction is catalysed with the immobilized $TiO_2$, however, the oxidation reaction is expected to take place in both, the functionalized wall by direct oxidation and in the liquid slugs by oxidation with reactive species in the liquid (i.e. hydroxyl radicals, non-stable intermediates, dissolved oxygen radicals, etc.).

FIGURE 13

There is included as supplementary material a chromatogram of a mixture of standard samples (S1). Retention times of compounds of interest are summarized in table S1 and a representative chromatogram of a reaction sample is provided also as supplementary material (S2).

Finally, it is worth emphasizing that regardless the small reactor volume assessed here and the relative low mineralization percentages attained, this type of reactor could be of practical use by scaling them up (making them longer and slightly wider) or by scaling them out (placing thousands of them in parallel with a gas distributor or inside a bubble column) [11]. Also, it is important to bear on mind that the radiation source used in this work was rather energetic. This is definitely an issue that is worth addressing in future related works.

## 4. Conclusions

Quartz capillaries were coated with $TiO_2$ (anatase) films by sol-gel method and they performance as photo-reactors was assessed by carrying out the three-phase photocatalyzed oxidation of 2-DHBA under UV light. The initial reaction rate was found be dependant on the dilution degree of the precursor sol and on the number of coating cycles. The maximum reaction rate ($106.32 \times 10^{-6}$ mol $dm^{-3}s^{-1}$) was achieved when using a precursors volumetric ratio of 1:15:1 and two coating cycles. It was found that the capillary channels are suitable to be reused due to strong adherence of the film to the substrate. Finally, it can be concluded that photo-capillary reactors allow tuning the products distribution by using the catalyst either in slurry or immobilized onto the capillary reactor wall. Therefore this type of reactors can be utilized to conduct either type of photo-catalytic process, advanced or selective oxidation. The photonic efficiency is significantly increased (about three orders of magnitude) when the catalyst is immobilized onto the capillary reactor compared to the slurry STR. The use of the capillary reactor as slurry reactor also offers a photon efficiency improvement (about one order of magnitude) compared to a typical slurry STR.

Acknowledgements

L. Hurtado acknowledges CONACYT-Mexico the scholarship No. 56499. Project PRODEP for advanced oxidation processes is also acknowledged for financial support. Citlalit Martinez Soto technical support is also acknowledged.

REFERENCES

[1] M.R. Hoffmann, S.T. Martin, W. Choi, D.W. Bahnemann, Environmental Applications of Semiconductor Photocatalysis, Chemical Reviews 95 (1995) 69-96.

[2] T.E. Doll, F.H. Frimmel, Removal of selected persistent organic pollutants by heterogeneous photocatalysis in water, Catalysis Today 101 (2005) 195-202.

[3] A. Di Paola, E. García-López, G. Marcì, L. Palmisano, A survey of photocatalytic materials for environmental remediation, Journal of Hazardous Materials 211–212 (2012) 3-29.

[4] K. Kabra, R. Chaudhary, R.L. Sawhney, Treatment of Hazardous Organic and Inorganic Compounds through Aqueous-Phase Photocatalysis: A Review, Ind. Eng. Chem. Res. 43 (2004) 7683-7696.

[5] V. Augugliaro, G. Camera-Roda, V. Loddo, G. Palmisano, L. Palmisano, F. Parrino, M.A. Puma, Synthesis of vanillin in water by TiO2 photocatalysis, Applied Catalysis B: Environmental 111–112 (2012) 555-561.

[6] M. Bellardita, V. Loddo, G. Palmisano, I. Pibiri, L. Palmisano, V. Augugliaro, Photocatalytic green synthesis of piperonal in aqueous TiO2 suspension, Applied Catalysis B: Environmental 144 (2014) 607-613.

[7] J. Schneider, D. Bahnemann, J. Ye, G.L. Puma, D.D. Dionysiou, Photocatalysis: Fundamentals and Perspectives, Royal Society of Chemistry2016.

[8] Y. Matsushita, S. Kumada, K. Wakabayashi, K. Sakeda, T. Ichimura, Photocatalytic Reduction in Microreactors, ChemInform 37 (2006) no-no.

[9] Y. Matsushita, T. Ichimura, N. Ohba, S. Kumada, K. Sakeda, T. Suzuki, H. Tanibata, T. Murata, Recent progress on photoreactions in microreactors, Pure and Applied Chemistry 79 (2007).

[10] M.T. Kreutzer, F. Kapteijn, J.A. Moulijn, J.J. Heiszwolf, Multiphase monolith reactors: Chemical reaction engineering of segmented flow in microchannels, Chemical Engineering Science 60 (2005) 5895-5916.

[11] R. Natividad, J. Cruz-Olivares, R.P. Fishwick, J. Wood, J.M. Winterbottom, Scaling-out selective hydrogenation reactions: From single capillary reactor to monolith, Fuel 86 (2007) 1304-1312.

[12] D. Russo, D. Spasiano, M. Vaccaro, R. Andreozzi, G. Li Puma, N.M. Reis, R. Marotta, Direct photolysis of benzoylecgonine under UV irradiation at 254 nm in a continuous flow microcapillary array photoreactor, Chemical Engineering Journal 283 (2016) 243-250.

[13] H. Fujiwara, H. Hosokawa, K. Murakoshi, Y. Wada, S. Yanagida, T. Okada, H. Kobayashi, Effect of Surface Structures on Photocatalytic CO2 Reduction Using Quantized CdS Nanocrystallites, The Journal of Physical Chemistry B 102 (1998) 4440-4440.

[14] Z.S. Khalifa, H. Lin, S. Ismat Shah, Structural and electrochromic properties of TiO2 thin films prepared by metallorganic chemical vapor deposition, Thin Solid Films 518 (2010) 5457-5462.

[15] M.O. Abou-Helal, W.T. Seeber, Preparation of TiO2 thin films by spray pyrolysis to be used as a photocatalyst, Applied Surface Science 195 (2002) 53-62.

[16] L. Escobar-Alarcón, E. Haro-Poniatowski, M.A. Camacho-López, M. Fernández-Guasti, J. Jímenez-Jarquín, A. Sánchez-Pineda, Structural characterization of TiO2 thin films obtained by pulsed laser deposition, Applied Surface Science 137 (1999) 38-44.

[17] L. Hu, T. Yoko, H. Kozuka, S. Sakka, Effects of solvent on properties of sol—gel-derived TiO2 coating films, Thin Solid Films 219 (1992) 18-23.

[18] D. Solís-Casados, L. Escobar-Alarcón, M. Fernández, F. Valencia, Malachite green degradation in simulated wastewater using Nix:TiO2 thin films, Fuel 110 (2013) 17-22.

[19] M. Tian, B. Adams, J. Wen, R. Matthew Asmussen, A. Chen, Photoelectrochemical oxidation of salicylic acid and salicylaldehyde on titanium dioxide nanotube arrays, Electrochimica Acta 54 (2009) 3799-3805.

[20] A. Mills, C.E. Holland, R.H. Davies, D. Worsley, Photomineralization of salicylic acid: a kinetic study, Journal of Photochemistry and Photobiology A: Chemistry 83 (1994) 257-263.

[21] K. Karthik, S.K. Pandian, N.V. Jaya, Effect of nickel doping on structural, optical and electrical properties of TiO2 nanoparticles by sol–gel method, Applied Surface Science 256 (2010) 6829-6833.

[22] W.-X. Xu, S. Zhu, X.-C. Fu, Q. Chen, The structure of TiOx thin film studied by Raman spectroscopy and XRD, Applied Surface Science 148 (1999) 253-262.

[23] A.M. Goodman, Optical interference method for the approximate determination of refractive index and thickness of a transparent layer, Appl. Opt. 17 (1978) 2779-2787.

[24] S.H. Mohamed, E.R. Shaaban, Microstructural, optical and photocatalytic properties of CdS doped TiO2 thin films, Physica B: Condensed Matter 406 (2011) 4327-4331.

[25] J. Tauc, R. Grigorovici, A. Vancu, Optical Properties and Electronic Structure of Amorphous Germanium, physica status solidi (b) 15 (1966) 627-637.

[26] F. Gassim, A.N. Alkhateeb, F.H. Hussein, Photocatalytic oxidation of benzyl alcohol using pure and sensitized anatase, Desalination 209 (2007) 342-349.

[27] K. Chhor, J.F. Bocquet, C. Colbeau-Justin, Comparative studies of phenol and salicylic acid photocatalytic degradation: influence of adsorbed oxygen, Materials Chemistry and Physics 86 (2004) 123-131.

FIGURE CAPTIONS

Figure 1. Chemical structure of salicylic acid (SA) or 2-dihidroxibenzoic acid (2-DHBA)

Figure 2. Capillary reactor system configuration

Figure 3. SEM images of films prepared at volumetric ratio i-PrO:2-propanol:$HNO_3$: A-1:5:0.5; B-1:25:1; C-1:50:1

Figure 4. SEM image of quartz capillary coated with $TiO_2$ film prepared with a volumetric proportion (i-PrO:2-propanol:$HNO_3$) 1:15:1

Figure 5. Raman spectra of $TiO_2$ films samples as function of volumetric ratio of precursors i-PrO:2-propanol:$HNO_3$

Figure 6. Transmittance spectra of a $TiO_2$ film and the substrate. Precursors volumetric ratio equal to 1:15:1

Figure 7. Tauc plot for estimation of band gap energy of $TiO_2$ film. Precursors volumetric ratio equal to 1:15:1

Figure 8. Flowmap of hydrodynamic regimes as function of dimensionless groups. System 2-DHBA-$O_2$; T=35°C; Capillary channel internal diameter = 0.003 m.

Figure 9. Typical absorbance spectra of the 2-DHBA degradation ($C_0$=100 ppm) during an experiment conducted in a $TiO_2$ coated capillary reactor. $TiO_2$ film with precursors volumetric ratio equal to 1:15:1. $u_L$=0.0089 m $s^{-1}$; $u_G$=0.0165 m $s^{-1}$; reaction volume: 45 mL; T=35°C. Samples were withdrawn each 30 minutes.

Figure 10. Initial reaction rate of degradation of salicylic acid as function of precursor sol composition

Figure 11. Influence of number of coating cycles on initial reaction rate of 2-DHBA oxidation. Precursors volumetric ratio equal to 1:15:1

Figure 12. Initial oxidation rate of 2-DHBA: Comparison of reaction system configuration. STR: $TiO_2$ Degussa P25 concentration=0.5 g $L^{-1}$; Capillary (Slurry): $TiO_2$ Degussa P25 concentration: 0.5 g $L^{-1}$; Capillary (Film): $TiO_2$ film with precursors volumetric ratio 1:15:1 and two coating cycles.

Figure 13. Effect of operating mode (slurry or immobilized catalyst) on selectivity when the reaction is conducted in a capillary reactor. Reaction time= 120 min, reaction volume=45 mL.

FIGURE 1

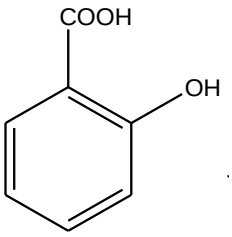


Salicylic acid

FIGURE 2

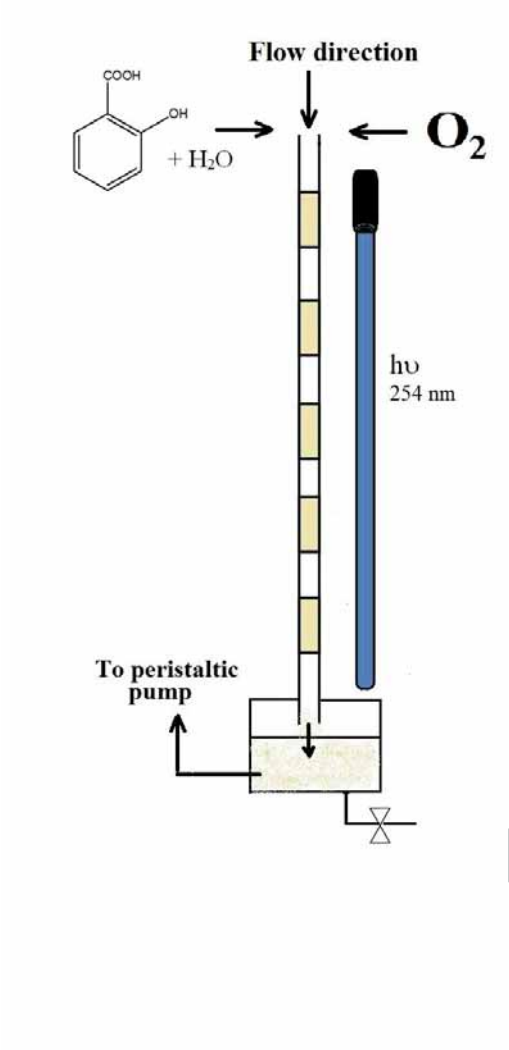

FIGURE 3

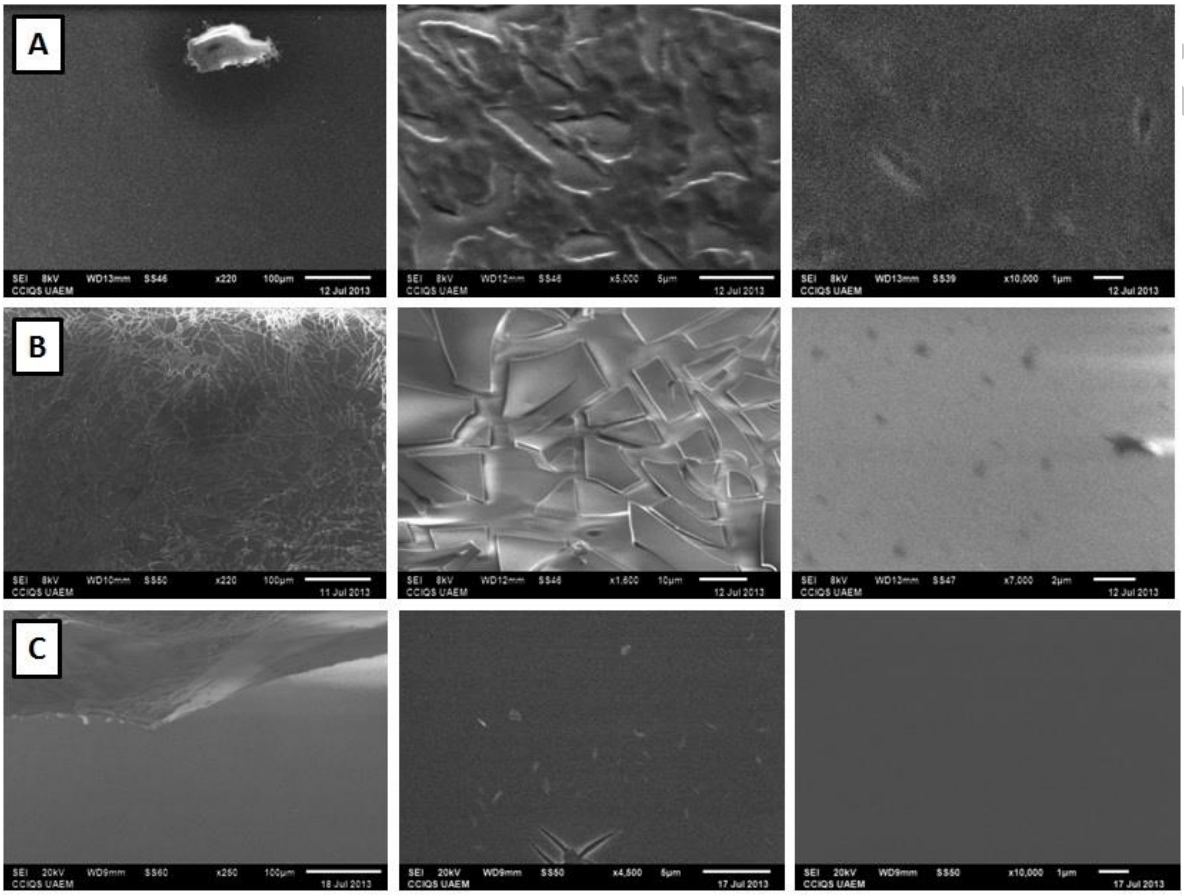

FIGURE 4

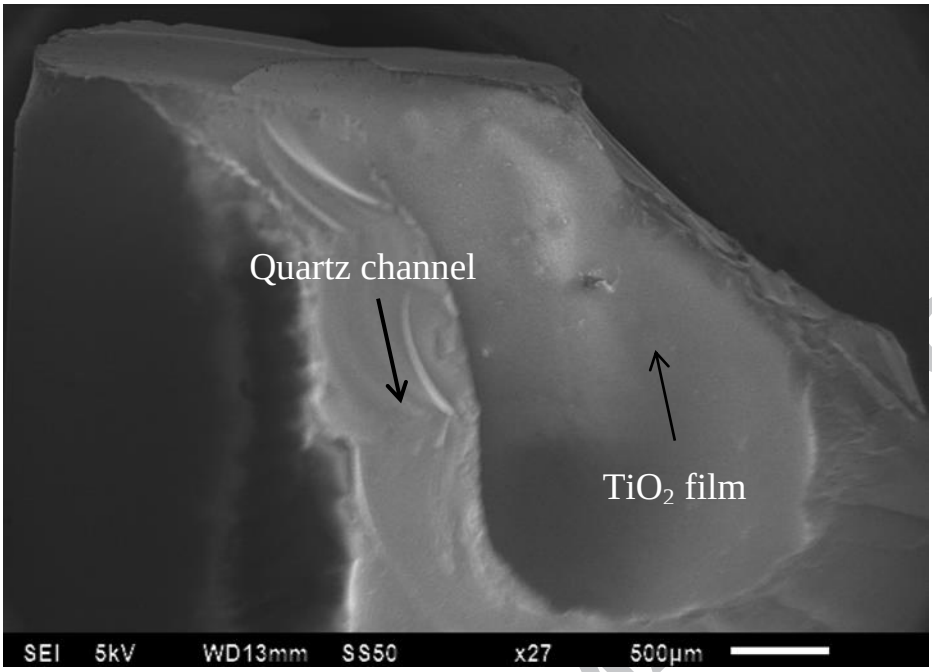

FIGURE 5

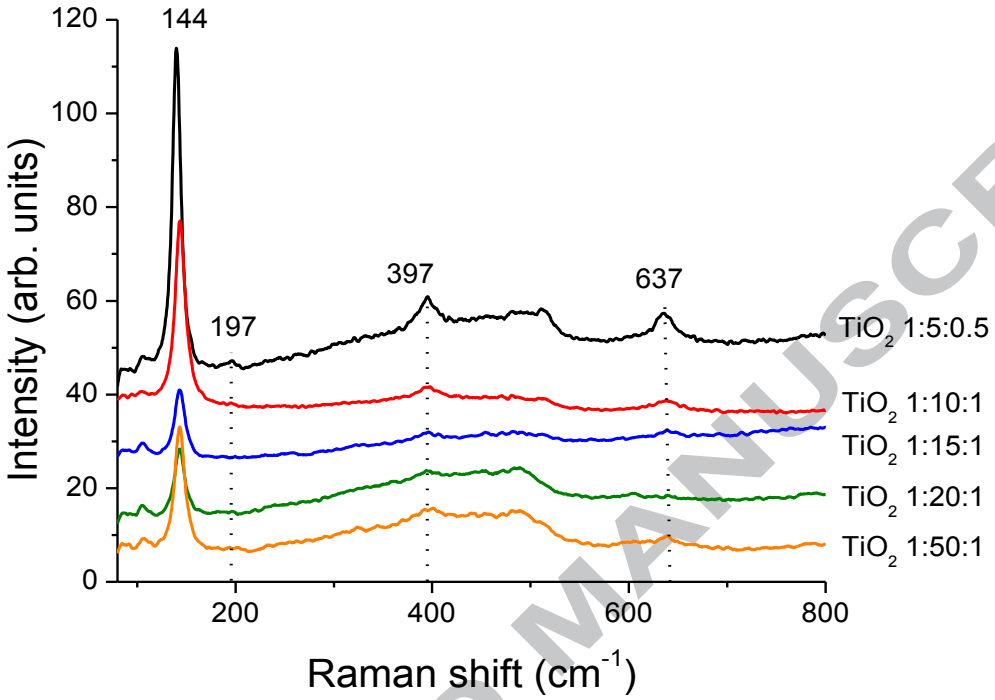

FIGURE 6

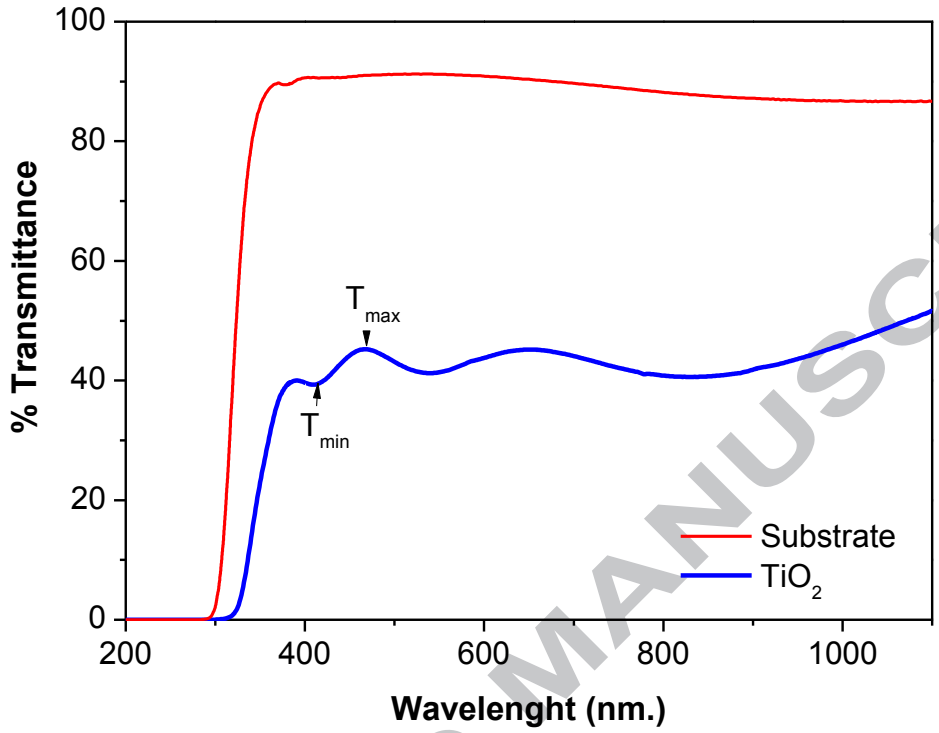

FIGURE 7

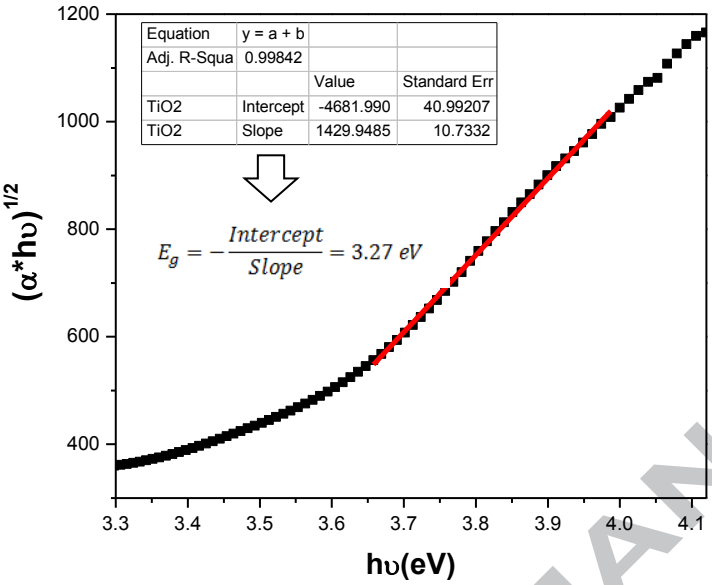

FIGURE 8

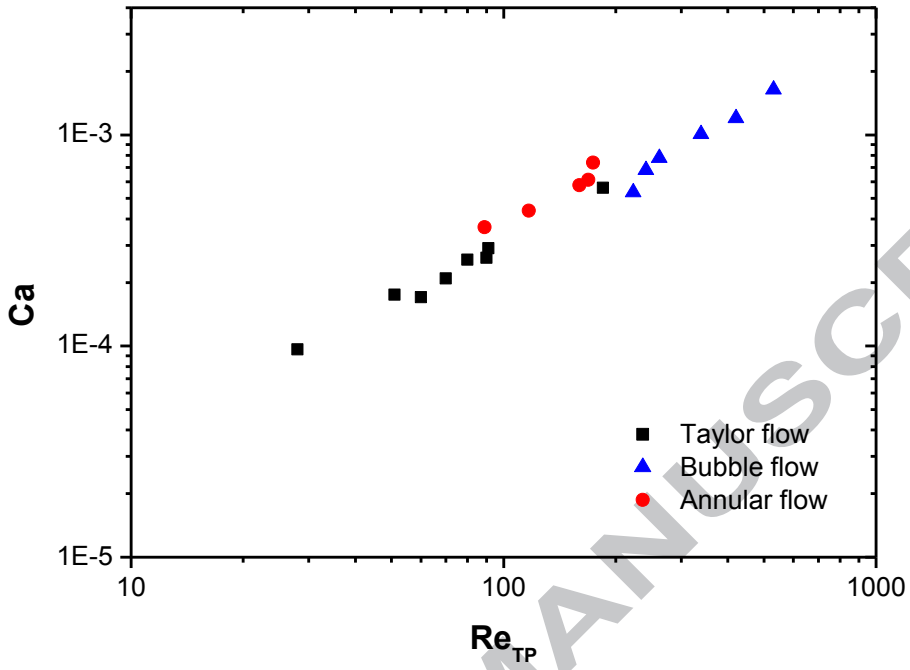

FIGURE 9

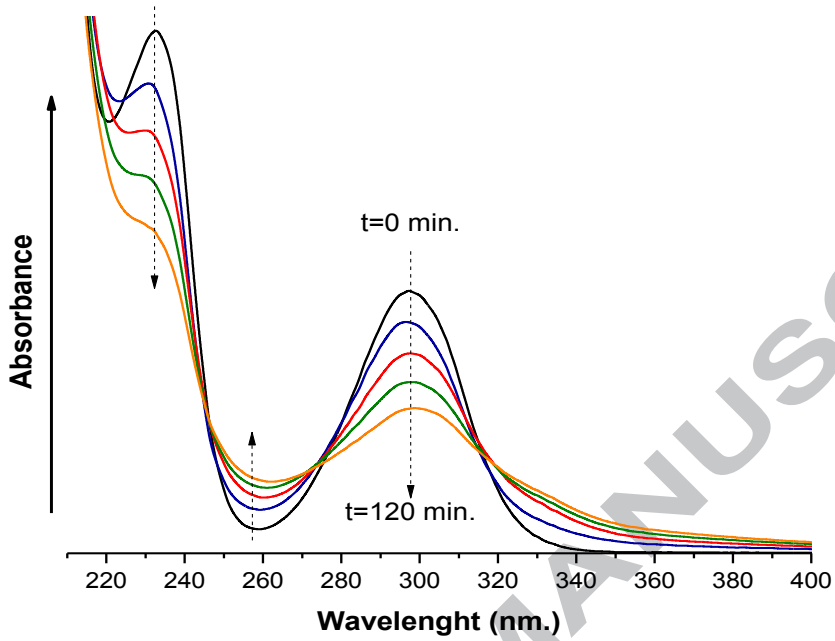

FIGURE 10

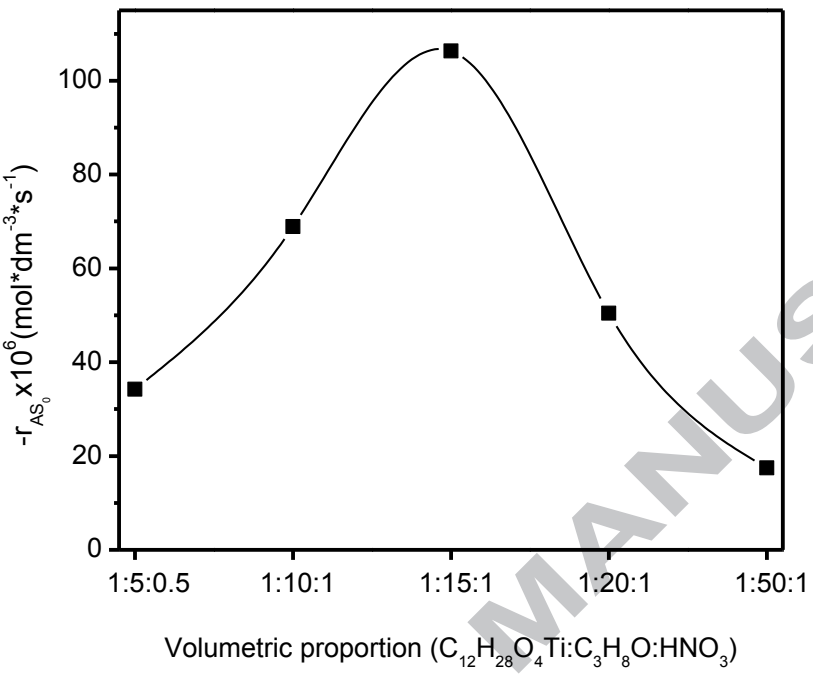

FIGURE 11

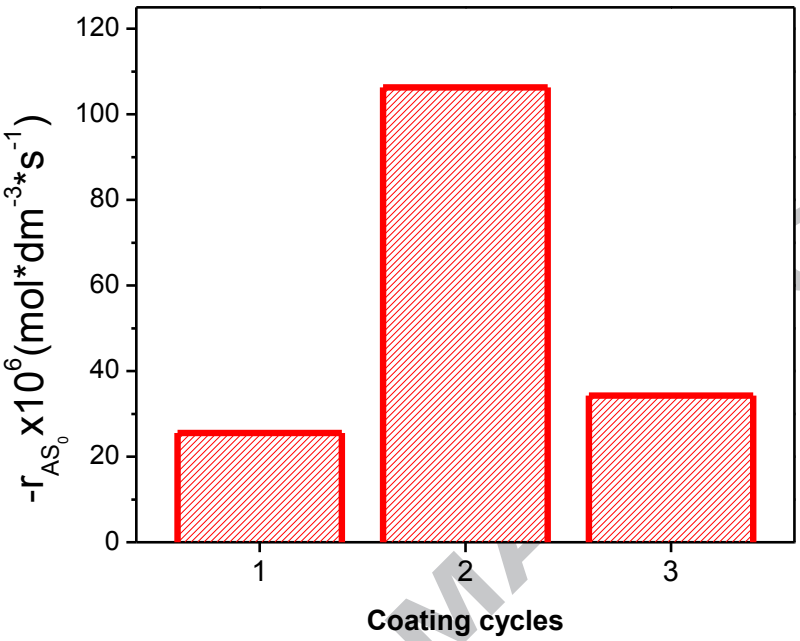

FIGURE 12

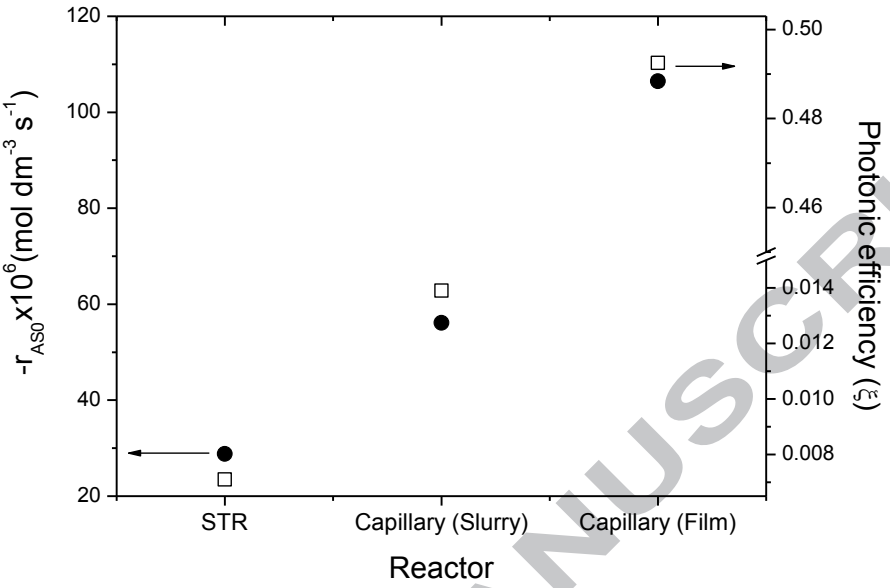

FIGURE 13

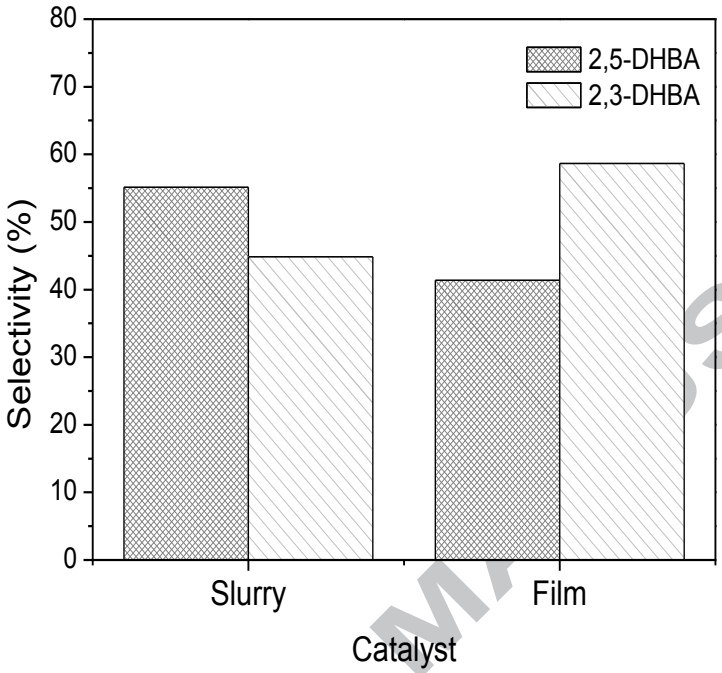

GRAPHICAL ABSTRACT

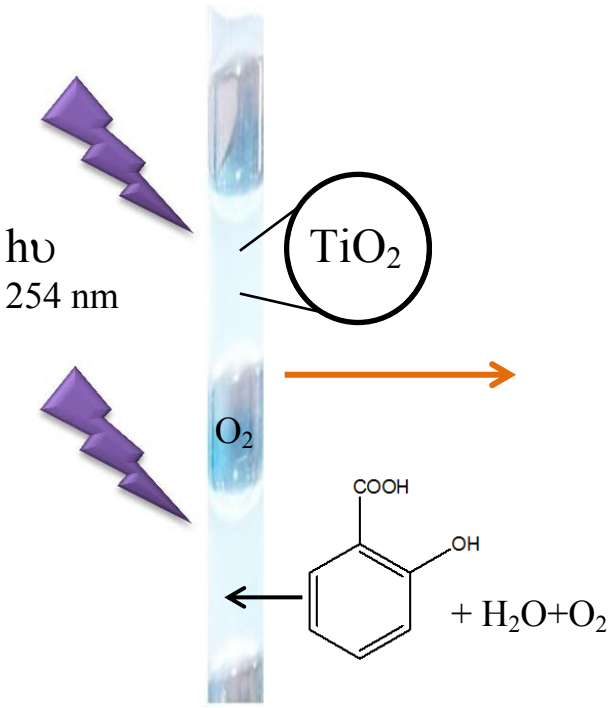


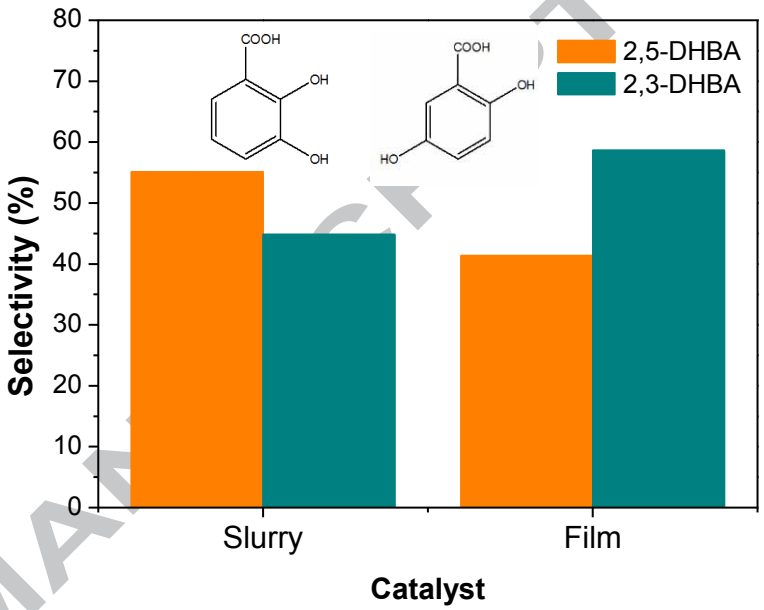

Highlights

- Quartz capillaries were coated with $TiO_2$ films by sol-gel method
- $TiO_2$ coated capillaries were assessed as multiphase photocatalytic reactors
- $TiO_2$ film precursors volumetric ratio and number of coating cycles affect oxidation rate
- A multiphase photocatalytic capillary reactor allows tuning product distribution